



TESS Data Release Notes:

Sector 42, DR60

*Michael M. Fausnaugh, Christopher J. Burke
Kavli Institute for Astrophysics and Space Science, Massachusetts Institute of Technology,
Cambridge, Massachusetts*

*Douglas A. Caldwell
SETI Institute, Mountain View, California*

*Jon M. Jenkins
NASA Ames Research Center, Moffett Field, California*

*Jeffrey C. Smith, Joseph D. Twicken
SETI Institute, Mountain View, California*

*Roland Vanderspek
Kavli Institute for Astrophysics and Space Science, Massachusetts Institute of Technology,
Cambridge, Massachusetts*

*John P. Doty
Noqi Aerospace Ltd, Billerica, Massachusetts*

*Eric B. Ting
NASA Ames Research Center, Moffett Field, California*

*Joel S. Villaseñor
Kavli Institute for Astrophysics and Space Science, Massachusetts Institute of Technology,
Cambridge, Massachusetts*

NASA STI Program ... in Profile

Since its founding, NASA has been dedicated to the advancement of aeronautics and space science. The NASA scientific and technical information (STI) program plays a key part in helping NASA maintain this important role.

The NASA STI program operates under the auspices of the Agency Chief Information Officer. It collects, organizes, provides for archiving, and disseminates NASA's STI. The NASA STI program provides access to the NTRS Registered and its public interface, the NASA Technical Reports Server, thus providing one of the largest collections of aeronautical and space science STI in the world. Results are published in both non-NASA channels and by NASA in the NASA STI Report Series, which includes the following report types:

- **TECHNICAL PUBLICATION.** Reports of completed research or a major significant phase of research that present the results of NASA Programs and include extensive data or theoretical analysis. Includes compilations of significant scientific and technical data and information deemed to be of continuing reference value. NASA counterpart of peer-reviewed formal professional papers but has less stringent limitations on manuscript length and extent of graphic presentations.
- **TECHNICAL MEMORANDUM.** Scientific and technical findings that are preliminary or of specialized interest, e.g., quick release reports, working papers, and bibliographies that contain minimal annotation. Does not contain extensive analysis.
- **CONTRACTOR REPORT.** Scientific and technical findings by NASA-sponsored contractors and grantees.

- **CONFERENCE PUBLICATION.** Collected papers from scientific and technical conferences, symposia, seminars, or other meetings sponsored or co-sponsored by NASA.
- **SPECIAL PUBLICATION.** Scientific, technical, or historical information from NASA programs, projects, and missions, often concerned with subjects having substantial public interest.
- **TECHNICAL TRANSLATION.** English-language translations of foreign scientific and technical material pertinent to NASA's mission.

Specialized services also include organizing and publishing research results, distributing specialized research announcements and feeds, providing information desk and personal search support, and enabling data exchange services.

For more information about the NASA STI program, see the following:

- Access the NASA STI program home page at <http://www.sti.nasa.gov>
- E-mail your question to help@sti.nasa.gov
- Phone the NASA STI Information Desk at 757-864-9658
- Write to:
NASA STI Information Desk
Mail Stop 148
NASA Langley Research Center
Hampton, VA 23681-2199



TESS Data Release Notes: Sector 42, DR60

*Michael M. Fausnaugh, Christopher J. Burke
Kavli Institute for Astrophysics and Space Science, Massachusetts Institute of Technology,
Cambridge, Massachusetts*

*Douglas A. Caldwell
SETI Institute, Mountain View, California*

*Jon M. Jenkins
NASA Ames Research Center, Moffett Field, California*

*Jeffrey C. Smith, Joseph D. Twicken
SETI Institute, Mountain View, California*

*Roland Vanderspek
Kavli Institute for Astrophysics and Space Science, Massachusetts Institute of Technology,
Cambridge, Massachusetts*

*John P. Doty
Noqi Aerospace Ltd, Billerica, Massachusetts*

*Eric B. Ting
NASA Ames Research Center, Moffett Field, California*

*Joel S. Villaseñor
Kavli Institute for Astrophysics and Space Science, Massachusetts Institute of Technology,
Cambridge, Massachusetts*

Acknowledgements

These Data Release Notes provide information on the processing and export of data from the Transiting Exoplanet Survey Satellite (TESS). The data products included in this data release are full frame images (FFIs), target pixel files, light curve files, collateral pixel files, cotrending basis vectors (CBVs), and Data Validation (DV) reports, time series, and associated xml files.

These data products were generated by the TESS Science Processing Operations Center (SPOC, [Jenkins et al., 2016](#)) at NASA Ames Research Center from data collected by the TESS instrument, which is managed by the TESS Payload Operations Center (POC) at Massachusetts Institute of Technology (MIT). The format and content of these data products are documented in the [Science Data Products Description Document \(SDPDD\)](#)¹. The SPOC science algorithms are based heavily on those of the Kepler Mission science pipeline, and are described in the Kepler Data Processing Handbook ([Jenkins, 2020](#)).² The Data Validation algorithms are documented in [Twicken et al. \(2018\)](#) and [Li et al. \(2019\)](#). The [TESS Instrument Handbook](#) ([Vanderspek et al., 2018](#)) contains more information about the TESS instrument design, detector layout, data properties, and mission operations.

The TESS Mission is funded by NASA's Science Mission Directorate.

This report is available in electronic form at
<https://archive.stsci.edu/tess/>

¹<https://archive.stsci.edu/missions/tess/doc/EXP-TESS-ARC-ICD-TM-0014-Rev-F.pdf>

²<https://archive.stsci.edu/kepler/manuals/KSCI-19081-003-KDPH.pdf>

1 Observations

TESS Sector 42 observations include physical orbits 91 and 92 of the spacecraft around the Earth. Data collection was paused for 0.93 days between the orbits to download data. In total, there are 24.54 days of science data collected in Sector 42.

Table 1: Sector 42 Observation times

	UTC	TJD ^a	Cadence #
Orbit 91 start	2021-08-21 04:25:00	2447.68551	878566
Orbit 91 end	2021-09-02 19:16:59	2460.30495	887652
Orbit 92 start	2021-09-03 17:34:59	2461.23411	888321
Orbit 92 end	2021-09-15 15:46:59	2473.15911	896907

^a TJD = TESS JD = JD - 2,457,000.0

The spacecraft was pointing at RA (J2000): 13.0140°; Dec (J2000): 6.3337°; Roll: 292.8009°. See the TESS project [Sector 42 observation page](#)³ for the coordinates of the spacecraft pointing and center field-of-view of each camera. Fields-of-view for each camera can be found at the TESS Guest Investigator Office [observations status page](#).⁴ The detailed target list for both 2-minute and 20-second data, as well as the Guest Investigator target lists, can be found at the [Sector 42 observation page](#) and the [observations status page](#).

Sector 42 is the first TESS observation of the ecliptic plane.

1.1 Notes on Individual Targets

There are no issues with missing light curves or clipped apertures in the 20-second data products. There were 1013 targets chosen for 20-second cadence observations, consisting of all observable targets from the 20-second Candidate Target List and 400 PPA stars.

For the 2-minute cadence data, one bright star ($T_{\text{mag}} \lesssim 1.8$) with a large pixel stamp was not processed in the photometric pipeline. Target pixel files with original and calibrated pixel data are provided, but no light curves were produced. Note that the TPF files do not include a background correction for stars without light curves. The affected TIC ID is 306349516.

Two additional targets (2053193606 and 504952282) are blended with brighter saturated stars. No optimal apertures were assigned in these cases. A target pixel file with the original and calibrated pixel data is provided for each, but no light curves were produced.

Two targets (40041408 and 250976540) were affected by Jupiter on Camera 1 CCD 4, column 264 (see §3.1). The bright smear signal from Jupiter cannot be reliably calibrated, and the pipeline did not identify pixels suitable for background estimation in these pixel stamps. A target pixel file with the original and calibrated pixel data is provided for each target, but no light curves were produced.

Eight target stars (91329517, 91329515, 91329512, 522415725, 508850829, 376904847, 212957673, 176070741) are blended with comparably bright stars—the contaminating flux

³<https://tess.mit.edu/observations/sector-42>

⁴<https://heasarc.gsfc.nasa.gov/docs/tess/sector.html>

for these objects is very large, and the resulting photometry for such targets is expected to be unreliable.

One target star (610713314) is closely blended with brighter neighbors. In this case, the assigned aperture is disjoint and the resulting photometry is unreliable.

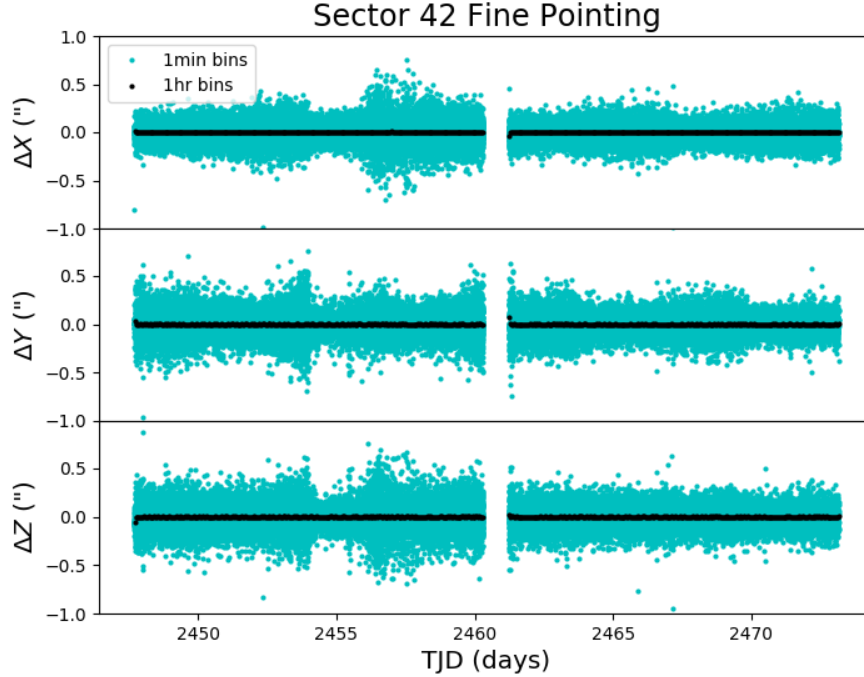


Figure 1: The delta-quaternions from each camera have been converted to spacecraft frame, binned to 1 minute and 1 hour, and averaged across cameras. Long-term trends (such as those caused by differential velocity aberration) have also been removed. The $\Delta X/\Delta Y$ directions represent offsets along the the detectors' rows/columns, while the ΔZ direction represents spacecraft roll.

1.2 Spacecraft Pointing and Momentum dumps

Sector 42 consists of observations of the ecliptic plane. For ecliptic pointings, the antisolar point is set towards the edge of Camera 1 (nearest Camera 2), and Cameras 2, 3, and 4 are aligned parallel to the ecliptic plane in the westward direction.

Camera 4 alone was used for guiding in orbits 91 and 92 of Sector 42. When the Moon crosses the field of view of Camera 4 at the end of orbit 91, there is almost no effect on the spacecraft's guiding performance (the pointing of the telescope changing by less than 0.01 pixels, 0.2 arcseconds). A single momentum dump was performed halfway through each orbit. Figure 1 summarizes the pointing performance over the course of the sector based on Fine Pointing telemetry.

1.3 Scattered Light

Figure 2 shows the median value of the background estimate for all targets on a given CCD as a function of time. Figure 3 shows the angle between each camera’s boresight and the Earth or Moon—this figure can be used to identify periods affected by scattered light and the relative contributions of the Earth and Moon to the image backgrounds.

In Orbit 91, the Moon crosses the fields of view of all cameras (one at a time), and the Earth crosses the fields of view of Cameras 1 and 2. The Moon and the Earth saturate CCD detectors during these times (see Figure 3; the camera fields of view are marked by the horizontal black line). Outside of these times, strong scattered light signals are also present for most of Orbit 91 and the second half of Orbit 92.

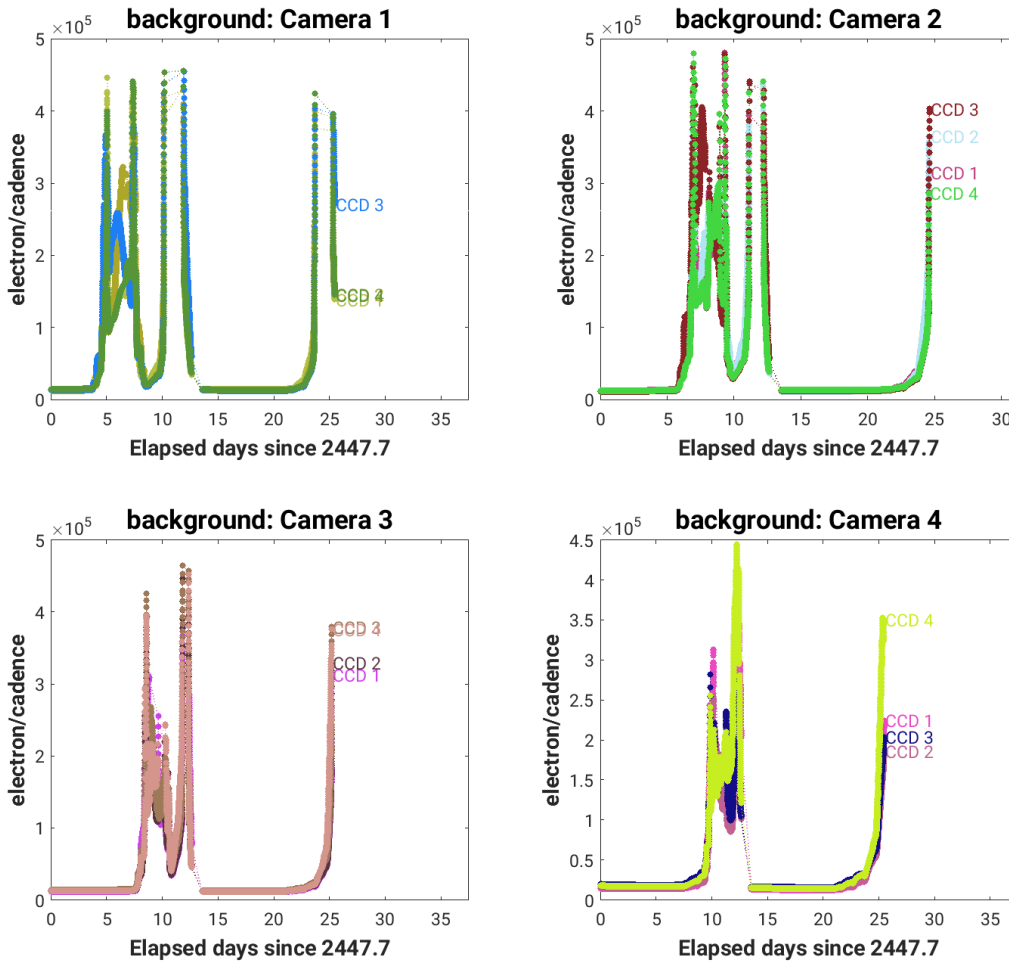


Figure 2: Median background flux across all targets on a given CCD in each camera. The changes are caused by variations in the orientation and distance of the Earth and Moon. In Sector 42, the Earth and Moon pass through the camera fields of view, saturating the detections.

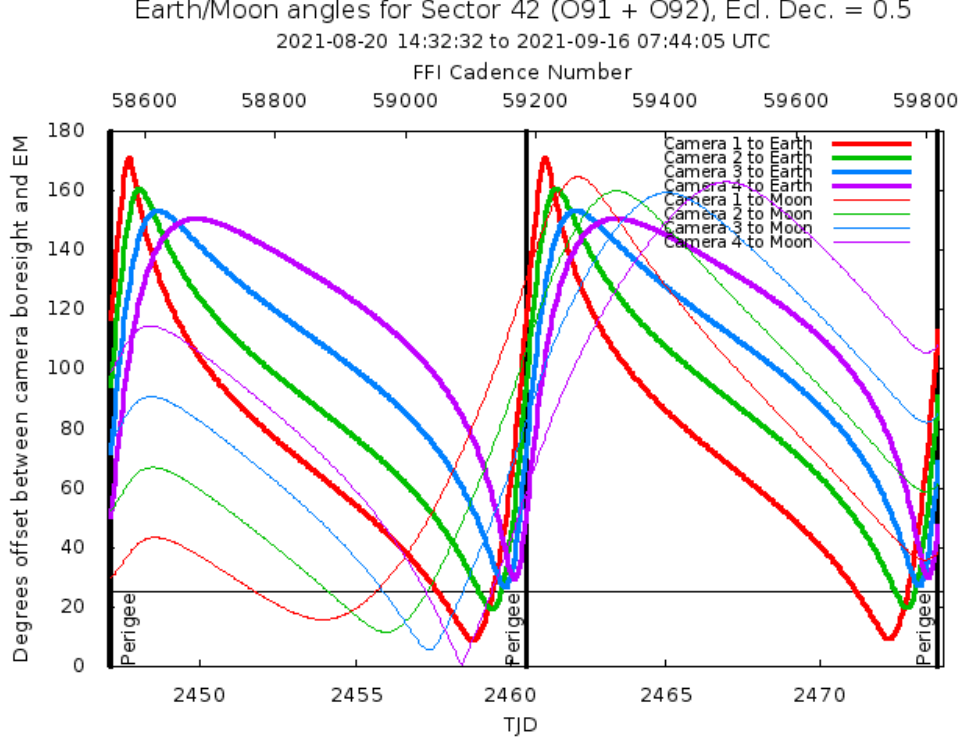


Figure 3: Angle between the four camera boresights and the Earth/Moon as a function of time. When the Earth is within $\sim 25^\circ$ of a camera’s boresight, transiting planet searches may be compromised by high levels of scattered light. At larger angles, up to $\sim 35^\circ$, scattered light patterns and complicated structures may be visible. At yet larger angles, low level patchy features may be visible. Scattered light from the Moon is generally only noticeable below $\sim 35^\circ$. This figure can be used to identify periods affected by scattered light and the relative contributions of the Earth and Moon to the background. However, the background intensity and locations of scattered light features depend on additional factors, such as the Earth/Moon azimuth and distance from the spacecraft.

2 Data Anomaly Flags

See the [SDPDD](#) (§9) for a list of data quality flags and the associated binary values used for TESS data, and the [TESS Instrument Handbook](#) for a more detailed description of each flag.

The following flags were not used in Sector 42: bits 1, 2, and 9 (Attitude Tweak, Safe Mode, and Discontinuity).

Cadences marked with bits 3, 4, 6, and 12 (Coarse Point, Earth Point, Reaction Wheel Desaturation Event, and Straylight) were marked based on spacecraft telemetry.

Cadences marked with bit 5 and 10 (Argabrightening Events and Impulsive Outlier) were identified by the SPOC pipeline. Bit 5 marks a sudden change in the background measurements. In practice, bit 5 flags are caused by rapidly changing glints and unstable pointing at times near momentum dumps. Bit 10 marks an outlier identified by PDC and omitted from the cotrending procedure.

The 20-second data mode includes cadences marked with bit 7 and 11 (Cosmic Ray

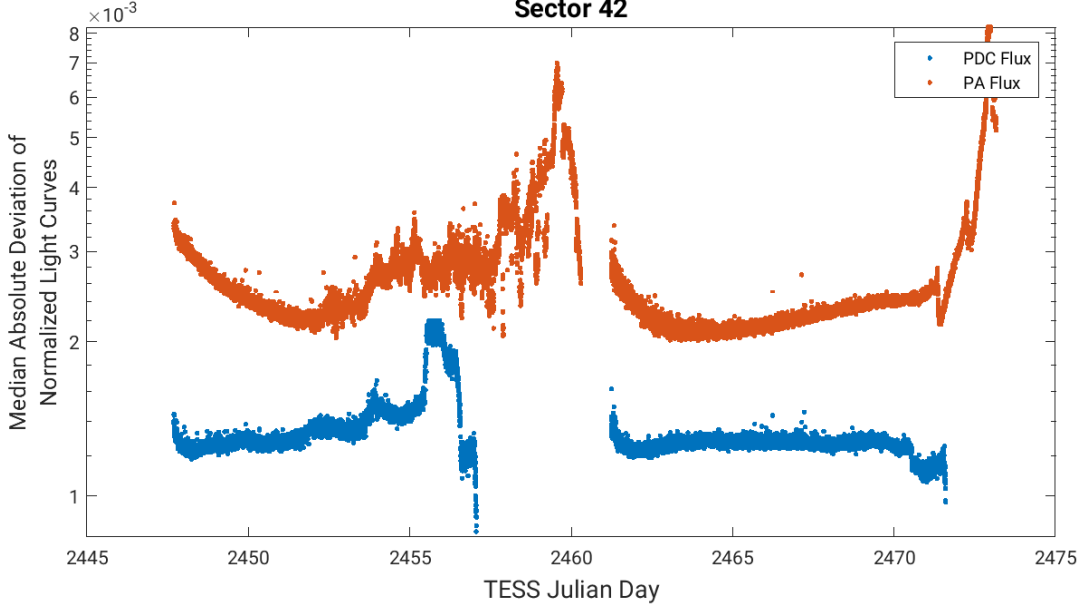


Figure 4: Median absolute deviation (MAD) for the two-minute cadence data from Sector 42, showing the performance of the cotrending after identifying Manual Exclude data quality flags. The MAD is calculated in each cadence across stars with flux variations less than 1% for both the PA (red) and PDC (blue) light curves, where each light curve is normalized by its median flux value. The scatter in the PA light curves is much higher than that for the PDC light curves, and the outliers in the PA light curves are largely absent from the PDC light curves due to the use of the anomaly flags.

in Optimal Aperture and Cosmic Ray in Collateral Pixel). These flags indicate cadences affected by cosmic rays that are removed by the pipeline, and can be found in both the TPF and LC files. The data provided in the archive products are corrected for cosmic rays, and a FITS table extension in the TPF and Collateral Pixel File details the cosmic rays identified and removed by the pipeline at the pixel level.

Cadences marked with bit 8 (Manual Exclude) are ignored by PDC, TPS, and DV for cotrending and transit searches. In Sector 42, these cadences were identified using spacecraft telemetry from the fine pointing system. All cadences with pointing excursions >7 arcsec (0.3 pixel) were flagged for manual exclude. Figure 4 also shows an assessment of the performance of the cotrending based on the final set of manual excludes.

The predicted stray light flag (bit 12, value 2048) is marked in the FFIs and flags times when the Earth/Moon are near the camera FOVs and may interfere with guiding or saturate the detectors. We strongly recommend that users inspect the FFI data before removing images marked with bit 12, because this bit is set based on predictions from mission planning and is known to be conservative with respect to the quality of data usable for analysis.

The predicted stray light flag (bit 12) is disabled for the 2-minute and 20-second data products. The scattered light exclude flag (bit 13, value 4096) identifies cadences at which individual targets are affected by scattered light

If the Earth/Moon interference is strong enough to saturate the detector, all targets on a CCD slice will be affected and the data are unusable. Cadences with bad calibrations due to

saturation are now explicitly marked with bit 15 (value 16384, “Bad Calibration Exclude”). For some cadences, the majority of targets on a CCD may be flagged for scattered light and not enough valid data remains to derive cotrending basis vectors in PDC. No systematic error correction can be applied at these times. This situation is identified by bit 16 (value 32768, “Insufficient Targets for Error Correction Exclude”).

FFIs were only marked with bits 3, 6, 8, 12, and 15 (Coarse Point, Reaction Wheel Desaturation Events, Manual Exclude, Straylight, and Bad Calibration Exclude). Only one FFI is affected by each momentum dump. There are no WCS coordinates for FFIs that coincide with momentum dumps.

3 Anomalous Effects

3.1 Jupiter

Jupiter was near opposition during Sector 42, and landed in the field-of-view of Camera 1 for ~ 7 days at the beginning of observations. Jupiter appears as a very bright object at the bottom of Camera 1, CCD 4, output channel A. It does not affect cotrending for any targets on this CCD, although the smear correction for its associated columns is unreliable and targets close to Jupiter may have unreliable photometry for the first 7 days of observations.

3.2 Smear Correction Issues

The following columns were impacted by bright stars in the science frame, and/or upper buffer rows, and/or lower science frame rows, which bleed into the upper serial register resulting in an overestimated smear correction. Whereas stars impact one to a few columns, the planet Jupiter impacts the smear correction over a band of columns (~ 50 pixels in width).

- Camera 1, CCD 1, Column 1533 - Star LQ Aquarii
- Camera 1, CCD 2, Column 1707 - Star Pi Aquarii
- Camera 1, CCD 4, Column 265 - Planet Jupiter
- Camera 2, CCD 1, Column 2067 - Star HD 491
- Camera 2, CCD 2, Column 339 - Star HD 43
- Camera 4, CCD 3, Column 1083 - Star BD+11 459
- Camera 4, CCD 3, Column 1818 - Star BD+16 410

4 Pipeline Performance and Results

4.1 Light Curves and Photometric Precision

Figure 5 gives the PDC goodness metrics for the two-minute cadence data, with residual correlation goodness and introduced noise goodness shown on a scale between 0 (bad) and 1

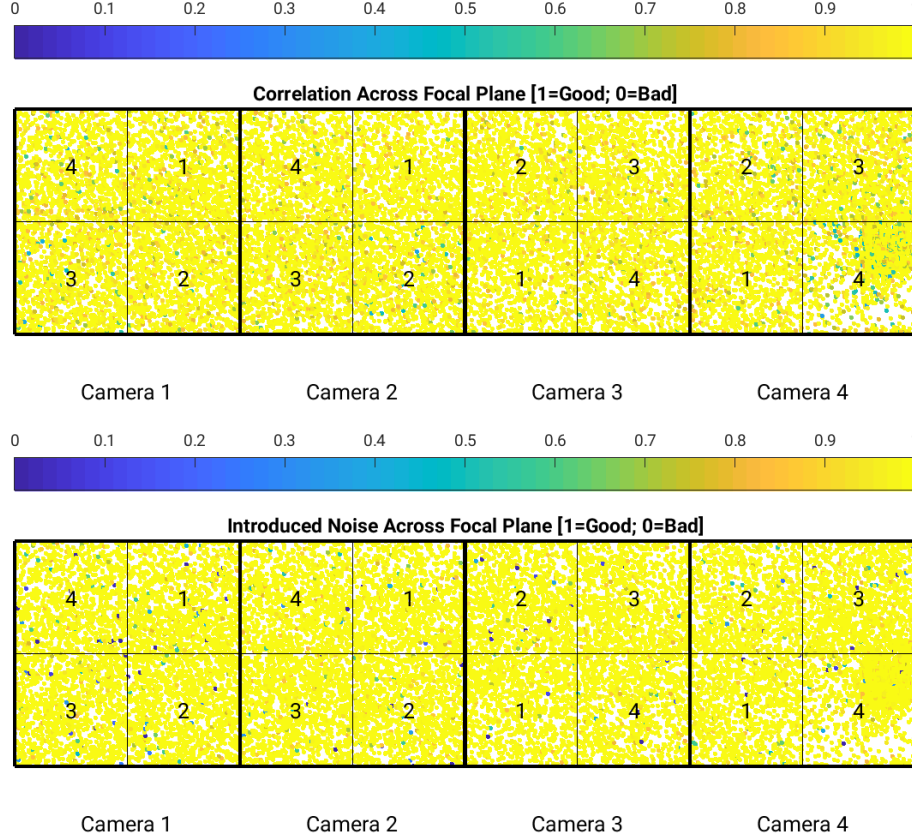


Figure 5: PDC residual correlation goodness metric (top panel) and PDC introduced noise goodness metric (bottom panel) for the two-minute cadence data. The metric values are shown on a focal plane map indicating the camera and CCD location of each target. The correlation goodness metric is calibrated such that a value greater than 0.8 means there is less than 10% mean absolute correlation between the target under study and all other targets on the CCD. The introduced noise metric is calibrated such that a value greater than 0.8 means the power in broad-band introduced noise is below the level of uncertainties in the flux values.

(good). The performance of PDC is very good and generally uniform over most of the field of view. Figure 6 shows the achieved Combined Differential Photometric Precision (CDPP) at 1-hour timescales for all two-minute targets.

4.2 Transit Search and Data Validation

In Sector 42, the two-minute light curves of 19995 targets were subjected to the transit search in TPS. Of these, Threshold Crossing Events (TCEs) at the 7.1σ level were generated for 792 targets.

We employed an iterative method when conducting the Sector 42 transit search. The top panel of Figure 7 shows the number of TCEs at a given cadence that exhibit a transit signal from an initial run of TPS. The $3\text{-}\sigma$ peaks were used to define de-emphasis weights for a second run of TPS, the results of which are shown in the bottom panel of Figure 7. The final set of TCEs and the results reported here are based on the second run of TPS. The

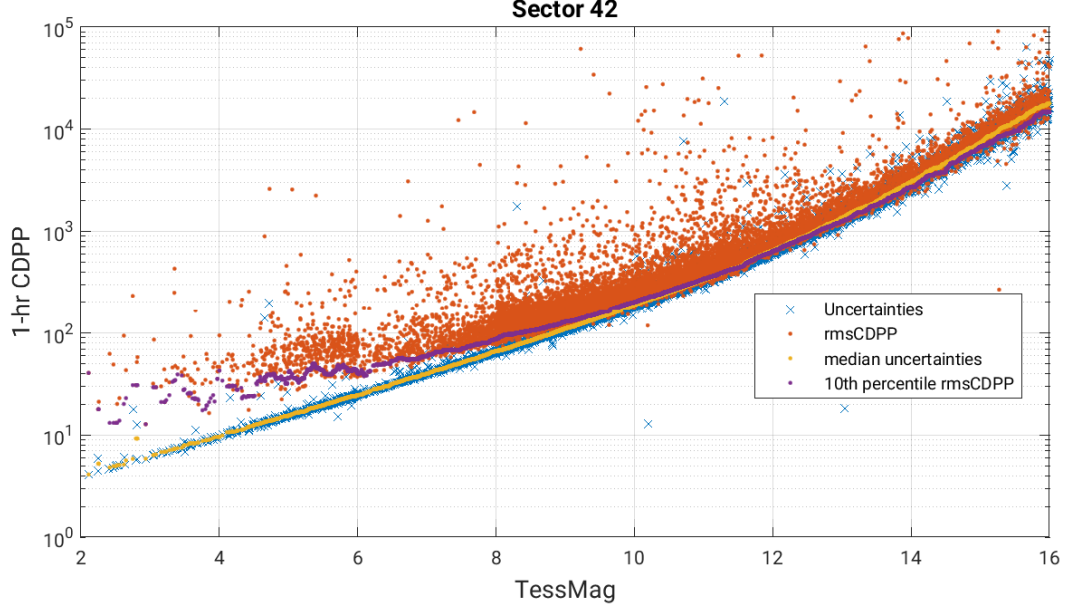


Figure 6: 1-hour CDPP. The red points are the RMS CDPP measurements for the 19995 light curves from Sector 42 plotted as a function of TESS magnitude. The blue x’s are the uncertainties, scaled to 1-hour timescale. The purple curve is a moving 10th percentile of the RMS CDPP measurements, and the gold curve is a moving median of the 1-hr uncertainties.

values of the adopted de-emphasis weights are provided in the DV timeseries data products for targets with TCEs.

The top panel of Figure 8 shows the distribution of orbital periods for the final set of TCEs found in Sector 42. There is a significant excess of TCEs with orbital period near 14 days due to scattered light in each orbit. The vertical histogram in the right panel of Figure 8 shows the distribution of transit depths derived from limb-darkened transiting planet model fits for TCEs. The model transit depths range down to the order of 100 ppm, but the bulk of the transit depths are considerably larger.

A search for additional TCEs in potential multiple planet systems was conducted in DV through calls to TPS. A total of 1023 TCEs were ultimately identified in the SPOC pipeline on 792 unique target stars. Table 2 provides a breakdown of the number of TCEs by target. Note that targets with large numbers of TCEs are likely to include false positives.

Table 2: Sector 42 TCE Numbers

Number of TCEs	Number of Targets	Total TCEs
1	621	621
2	126	252
3	33	99
4	9	36
5	3	15
—	792	1023

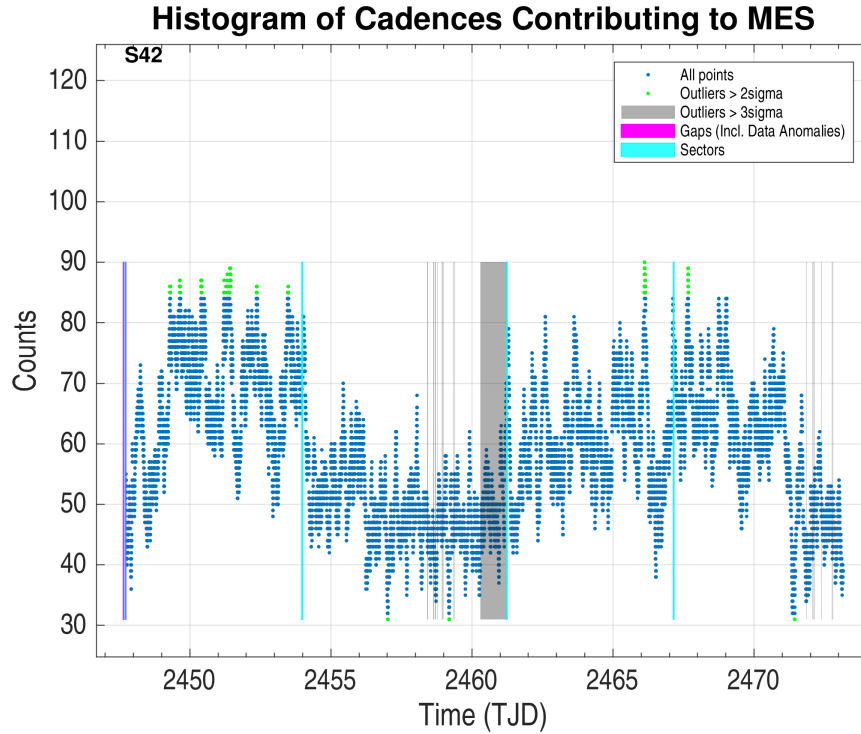
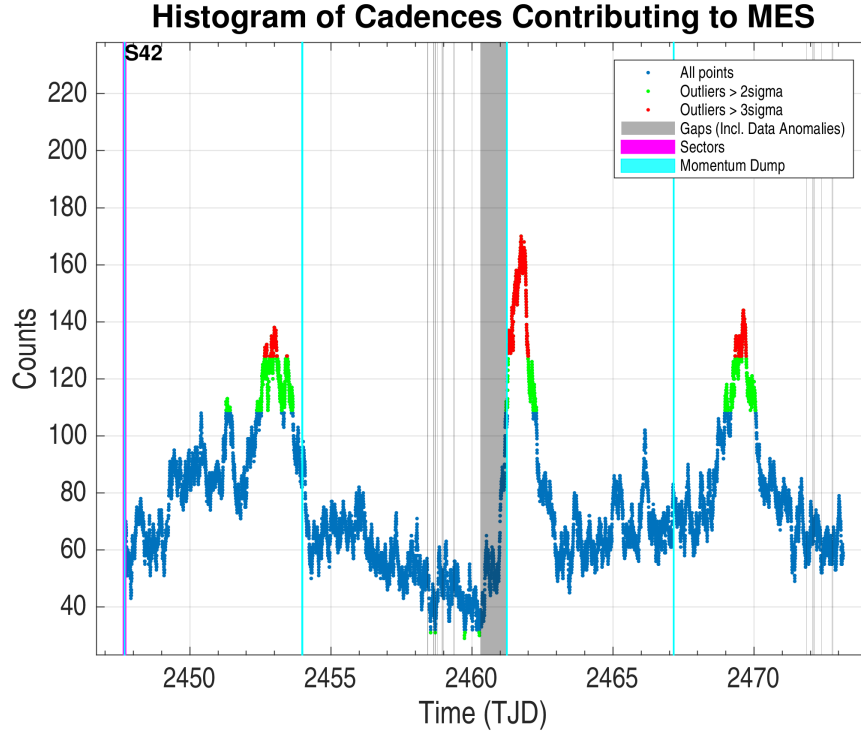


Figure 7: Top panel: Number of TCEs at a given cadence exhibiting a transit signal, based on an initial run of TPS. Any isolated peaks are caused by single events that result in spurious TCEs. These peaks were used to define de-emphasis weights that suppress problematic epochs for the transit detection statistics in a second iteration of TPS. Bottom panel: Results from the second run of TPS.

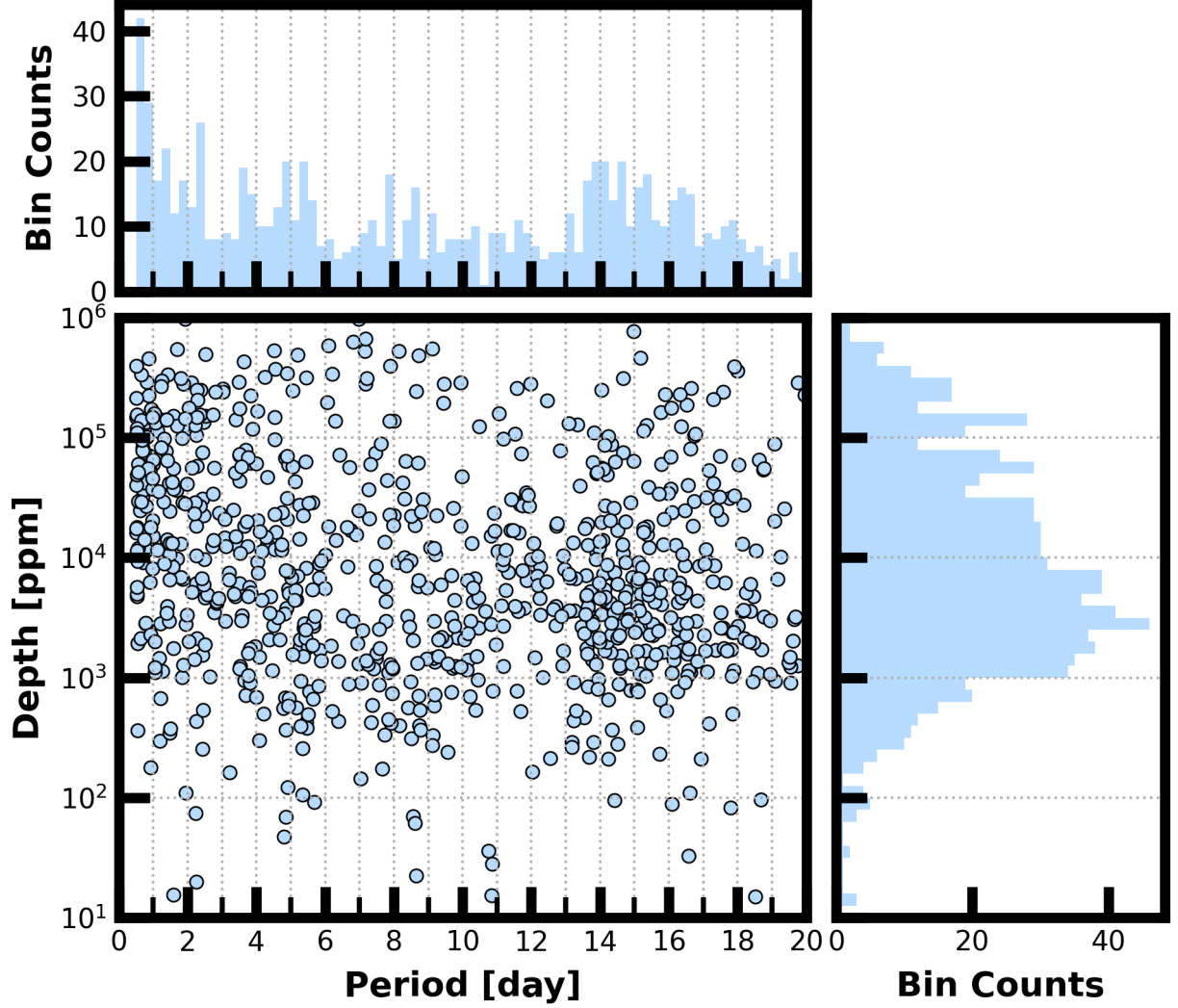


Figure 8: Lower Left Panel: Transit depth as a function of orbital period for the 1023 TCEs identified for the Sector 42 search. For enhanced visibility of long period detections, TCEs with orbital period < 0.5 days are not shown. Reported depth comes from the DV limb-darkened transit fit depth when available, and the DV trapezoid model fit depth when not available. Top Panel: Orbital period distribution of the TCEs shown in the lower left panel. Right Panel: Transit depth distribution for the TCEs shown in the lower left panel.

References

- Jenkins, J. M. 2020, [Kepler Data Processing Handbook](#): Overview of the Science Operations Center, Tech. rep., NASA Ames Research Center
- Jenkins, J. M., Twicken, J. D., McCauliff, S., et al. 2016, in Proc. SPIE, Vol. 9913, Software and Cyberinfrastructure for Astronomy IV, [99133E](#), doi: [10.1117/12.2233418](#)
- Li, J., Tenenbaum, P., Twicken, J. D., et al. 2019, *PASP*, 131, 024506, doi: [10.1088/1538-3873/aaf44d](#)
- Twicken, J. D., Catanzarite, J. H., Clarke, B. D., et al. 2018, *PASP*, 130, 064502, doi: [10.1088/1538-3873/aab694](#)
- Vanderspek, R., Doty, J., Fausnaugh, M., et al. 2018, [TESS Instrument Handbook](#), Tech. rep., Kavli Institute for Astrophysics and Space Science, Massachusetts Institute of Technology

Acronyms and Abbreviation List

BTJD Barycentric-corrected TESS Julian Date

CAL Calibration Pipeline Module

CBV Cotrending Basis Vector

CCD Charge Coupled Device

CDPP Combined Differential Photometric Precision

COA Compute Optimal Aperture Pipeline Module

CSCI Computer Software Configuration Item

CTE Charge Transfer Efficiency

Dec Declination

DR Data Release

DV Data Validation Pipeline Module

DVA Differential Velocity Aberration

FFI Full Frame Image

FIN FFI Index Number

FITS Flexible Image Transport System

FOV Field of View

FPG Focal Plane Geometry model

KDPH Kepler Data Processing Handbook

KIH Kepler Instrument Handbook

KOI Kepler Object of Interest

MAD Median Absolute Deviation

MAP Maximum A Posteriori

MAST Mikulski Archive for Space Telescopes

MES Multiple Event Statistic

NAS NASA Advanced Supercomputing Division

PA Photometric Analysis Pipeline Module

PDC Pre-Search Data Conditioning Pipeline Module

PDC-MAP Pre-Search Data Conditioning Maximum A Posteriori algorithm

PDC-msMAP Pre-Search Data Conditioning Multiscale Maximum A Posteriori algorithm

PDF Portable Document Format

POC Payload Operations Center

POU Propagation of Uncertainties

ppm Parts-per-million

PRF Pixel Response Function

RA Right Ascension

RMS Root Mean Square

SAP Simple Aperture Photometry

SDPDD Science Data Products Description Document

SNR Signal-to-Noise Ratio

SPOC Science Processing Operations Center

SVD Singular Value Decomposition

TCE Threshold Crossing Event

TESS Transiting Exoplanet Survey Satellite

TIC TESS Input Catalog

TIH TESS Instrument Handbook

TJD TESS Julian Date

TOI TESS Object of Interest

TPS Transiting Planet Search Pipeline Module

UTC Coordinated Universal Time

WCS World Coordinate System

XML Extensible Markup Language